

---

# Augmentation-aware Self-supervised Learning with Conditioned Projector

---

**Marcin Przewięzlikowski<sup>1,2,3</sup> \*** **Mateusz Pyla<sup>1,2,3</sup>** **Bartosz Zieliński<sup>1,3</sup>**  
**Bartłomiej Twardowski<sup>3,4</sup>** **Jacek Tabor<sup>1</sup>** **Marek Śmieja<sup>1</sup>**  
<sup>1</sup> Jagiellonian University, Faculty of Mathematics and Computer Science  
<sup>2</sup> Jagiellonian University, Doctoral School of Exact and Natural Sciences  
<sup>3</sup> IDEAS NCBR <sup>4</sup> Universitat Autònoma Barcelona

## Abstract

Self-supervised learning (SSL) is a powerful technique for learning robust representations from unlabeled data. By learning to remain invariant to applied data augmentations, methods such as SimCLR and MoCo are able to reach quality on par with supervised approaches. However, this invariance may be harmful to solving some downstream tasks which depend on traits affected by augmentations used during pretraining, such as color. In this paper, we propose to foster sensitivity to such characteristics in the representation space by modifying the projector network, a common component of self-supervised architectures. Specifically, we supplement the projector with information about augmentations applied to images. In order for the projector to take advantage of this auxiliary conditioning when solving the SSL task, the feature extractor learns to preserve the augmentation information in its representations. Our approach, coined **Conditional Augmentation-aware Self-supervised Learning (CASSLE)**, is directly applicable to typical joint-embedding SSL methods regardless of their objective functions. Moreover, it does not require major changes in the network architecture or prior knowledge of downstream tasks. In addition to an analysis of sensitivity towards different data augmentations, we conduct a series of experiments, which show that CASSLE improves over various SSL methods, reaching state-of-the-art performance in multiple downstream tasks.<sup>2</sup>

## 1 Introduction

Artificial neural networks have proven to be a successful family of models in several domains, including, but not limited to, computer vision [33], natural language processing [11], and solving problems at the human level with reinforcement learning [45]. This success is attributed largely to their ability to learn useful feature representations [29] without additional effort for input signals preparation. However, training large deep learning models requires extensive amounts of data, which can be costly to prepare, especially when human annotation is needed [3, 36].

High-quality image representations can be acquired without relying on explicitly labeled data by utilizing self-supervised learning (SSL). A self-supervised model is trained once on a large dataset without labels and then transferred to different downstream tasks. Initially, self-supervised methods addressed well-defined pretext tasks, such as predicting rotation [28] or determining patch position [22]. Recent studies in SSL proposed contrastive methods of learning representations that remain invariant when subjected to various data augmentations [32, 15, 18] leading to impressive results that have greatly diminished the disparity with representations learned in a supervised way [13].

---

\*Corresponding author: marcin.przewiezlikowski@doctoral.uj.edu.pl

<sup>2</sup>We share our codebase at <https://github.com/gmum/CASSLE>.

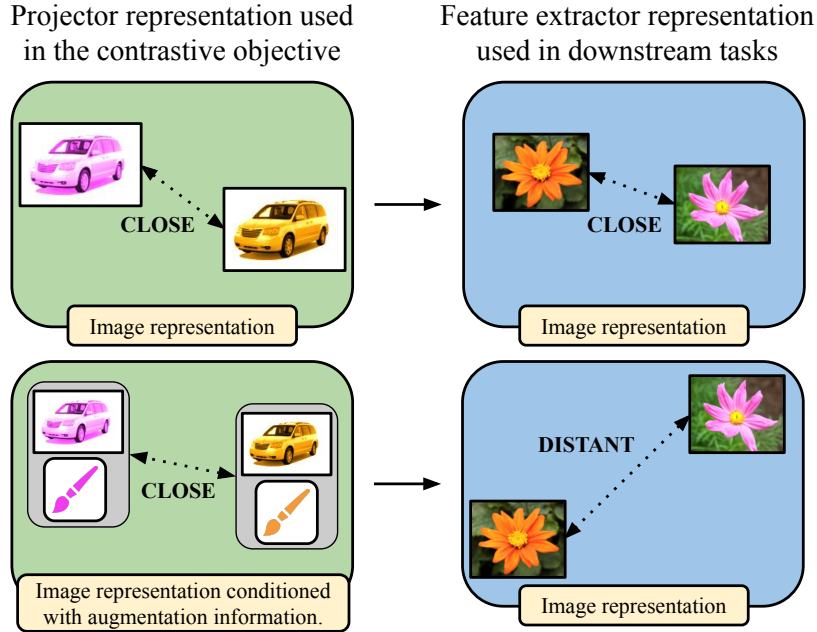


Figure 1: In the traditional self-supervised setting, contrastive loss minimization pulls the representations of augmented image views closer in the latent space of the projector (left). This may also reduce the distance between their feature extractor representations (right). Thus, the representation becomes invariant to augmentation-induced perturbations, which may hinder the performance on downstream tasks. In contrast, the self-supervised objective of CASSLE draws together joint representations of images and their augmentations in the projector space (bottom row). By conditioning the projector with augmentation information, image representations retain more sensitivity to perturbations in the feature extractor space. This proves to be beneficial when solving downstream tasks.

Nevertheless, contrastive methods may perform poorly when a particular downstream task relies on features affected by augmentation [69]. For example, color jittering can result in a representation space invariant to color shifts, which would be detrimental to the task of flower classification (see Figure 1). Without prior knowledge of possible downstream tasks, this effect is hard to mitigate in contrastive learning [62, 69]. Solutions for retaining information about used data augmentations in the feature extractor representation include forcing it explicitly with a modified training scheme [69, 40, 70], or by preparing a feature extractor to be adapted to a specific downstream task, e.g., with hypernetworks [14]. However, these approaches often involve significant modifications either to the contrastive model architecture [69], training procedure [40, 70], or costly training of additional models [14].

In this work, we propose a new method called **Conditional Augmentation-aware Self-supervised Learning (CASSLE)** that mitigates augmentation invariance of representation without neither major changes in network architecture or modifications to the self-supervised training objective. We propose to use the augmentation information during the SSL training as additional conditioning for the projector network. This encourages the feature extractor network to retain information about augmented image features in its representation. CASSLE can be applied to any joint-embedding SSL method regardless of its objective [17, 15, 18, 72, 19]. The outcome is a general-purpose, augmentation-aware encoder that can be directly used for any downstream task. CASSLE presents improved results in comparison to other augmentation-aware SSL methods, improving transferability to downstream tasks where invariance of the model representation for specific data changes could be harmful.

**The main contributions of our work are threefold:**

- We propose a simple yet effective method for Conditional Augmentation-aware Self-supervised Learning (CASSLE). Using our conditioned projector enables preserving more information about augmentations in representations than in existing methods.

- CASSLE is a general modification that can be directly applied to existing joint-embedding SSL approaches without introducing additional objectives and major changes in the network architecture.
- In a series of experiments we demonstrate that CASSLE reaches state-of-the-art performance with different SSL methods for robust representation learning and improves upon the performance of previous augmentation-aware approaches. Furthermore, our analysis indicates that CASSLE learns representations with increased augmentation sensitivity compared to other approaches.

## 2 Related work

**Self-supervised learning** (SSL) is a paradigm of learning representations from unlabeled data that can later be used for downstream tasks defined by human annotations [2, 4]. Despite learning artificial *pretext tasks*, instead of data-defined ones, SSL models have achieved tremendous success in a plethora of domains [21, 67, 60, 7]. This includes computer vision, where a variety of pretext tasks has been proposed [22, 74, 48, 28]. However, arguably the most prominent and successful SSL technique to emerge in recent years is the training of joint-embedding models for augmentation invariance [6, 64], defined by objectives such as contrastive InfoNCE loss [32, 15, 17], self-distillation [30, 15, 49] or Canonical Correlation Analysis [12, 72, 5]. Those objectives are often collectively referred to as *contrastive objectives* [63, 4]. A common component of joint-embedding architectures is the *projector network*, which maps representations of the feature extractor into the space where the contrastive objective is imposed [15, 17]. The usefulness of the projector has been explained through the lens of transfer learning, where it is often better to transfer intermediate network representations, to reduce the biases from the pretraining task [71, 9]. The projector also helps to mitigate the noisy data augmentations and enforces some degree of pairwise independence of image features [4, 44].

**Augmentation invariance of self-supervised models** is a natural consequence of training them with contrastive objectives, as SSL methods are prone to suppressing features that are not useful for optimizing the contrastive objectives [16, 57]. While a common set of augmentations demonstrated to typically work well on natural images in SSL has been established in the literature [32, 15, 18, 12, 75], the optimal choice of augmentations varies between specific tasks [62, 24]. [69] find that augmentation invariance can hinder the performance of the model on downstream tasks that require attention to precisely those traits that it had been previously trained to be invariant to. On the other hand, [73] observe that the objective of predicting augmentation parameters can be in itself a useful pretext task for SSL. Those works inspired several techniques of retaining augmentation-specific information in joint-embedding models, such as projectors sensitive to different augmentation types [69, 24], adding an objective of explicit prediction of augmentation parameters [40], , as well as task-specific pretraining [55, 65]. The above approaches produce general-purpose feature extractors that can be transferred to downstream tasks without further tuning of their parameters. However, they often involve complex modifications either to the SSL model architecture [69], training procedure [40, 70], or simply tedious task-specific pretraining [65]. Another line of work proposes to train Hypernetworks [31] which produce feature extractors invariant to chosen subsets of augmentations – a more elastic, but considerably harder to train approach [14]. Several works have proposed fostering the equivariance of representations to data transformations using augmentation information. [70] modulate the contrastive objective with augmentation strength, [8] use augmentation information as a signal for equivariance regularization in the supervised setting, whereas [27] extend the VicReg [5] objective with a predictor whose parameters are generated from augmentation information by a hypernetwork [31]. Compared to those works, we do not make any modifications to the objective functions of the extended approaches and evaluate CASSLE on a wide range of joint-embedding approaches and conditioning techniques. Following [69, 40], we produce a general-purpose feature extractor and utilize augmentation information similarly to [73, 40, 14]. Contrary to the above methods, we inject the information about the applied augmentations directly into the projector and make no modification either to the contrastive objective or the feature extractor.

## 3 Method

In this section, we present our approach, **Conditional Augmentation-aware Self-supervised learning** (CASSLE). Section 3.1 provides background on joint-embedding self-supervised methods and their limitations. Section 3.2 explains the essence of CASSLE and how it leverages augmentation

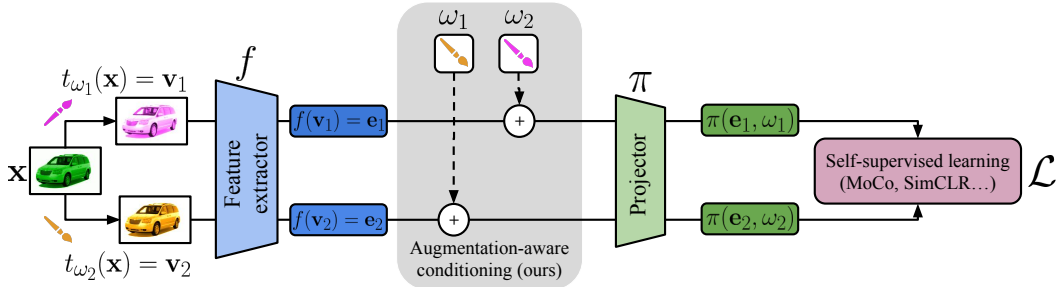


Figure 2: Overview of CASSLE. We extend the typical self-supervised learning approaches by incorporating the information of augmentations applied to images into the projector network. In CASSLE, the SSL objective is thus imposed on joint representations of images and the augmentations that had been applied to them. This way, CASSLE enables the feature extractor to be more aware of augmentations than the methods that do not condition the projector network.

information to improve the quality of learned representations. Section 3.3 details the practical implementation of CASSLE’s conditioning mechanism.

### 3.1 Preliminaries

A typical contrastive framework used in self-supervised learning consists of an augmentation function  $t_\omega$  and two networks: feature extractor  $f$  and projector  $\pi$ . Let  $v_1 = t_{\omega_1}(x)$ ,  $v_2 = t_{\omega_2}(x)$  be two augmentations of a sample  $x \sim X$  parameterized by  $\omega_1, \omega_2 \sim \Omega$ . The feature extractor maps them into the embedding space, which is the representation used in downstream tasks. To make the representation invariant to data augmentations,  $e_1 = f(v_1)$  is forced to be similar to  $e_2 = f(v_2)$ <sup>3</sup>. However, instead of imposing similarity constraints directly on the embedding space of  $f$ , a projector  $\pi$  transforms the embeddings into target space where the contrastive loss  $\mathcal{L}$  is applied. This trick, known as *Guillotine Regularization*, helps the feature extractor to better generalize to downstream tasks, due to  $f$  not being directly affected by  $\mathcal{L}$  [71, 15, 17, 9].

Minimizing  $\mathcal{L}(\pi(e_1), \pi(e_2))$  directly leads to reducing the distance between embeddings  $\pi(e_1)$  and  $\pi(e_2)$ . However,  $\mathcal{L}$  still indirectly encourages intermediate network representations (including the output of the feature extractor  $f$ ) to also conform to the contrastive objective to some extent. As a result, the feature extractor tends to erase the information about augmentation from its output representation. This behavior may however be detrimental for certain downstream tasks (see Figures 1 and 4), which rely on features affected by augmentations. For instance, learning invariance to color jittering through standard contrastive methods may lead to degraded performance on the downstream task of flower recognition, which is not a color-invariant task [62, 69]. Therefore, the success of typical SSL approaches depends critically on a careful choice of augmentations used for model pretraining [15, 62].

### 3.2 CASSLE

To overcome the above limitations of SSL, we facilitate the feature extractor to encode the information about augmentations in its output representation. In consequence, the obtained representation will be more informative for downstream tasks that depend on features modified by augmentations.

CASSLE achieves this goal by conditioning the projector  $\pi$  on the parameters of augmentations used to perturb the input image. Specifically, we modify  $\pi$  so that apart from embedding  $e$ , it also receives augmentation information  $\omega$  and projects their joint representation into the space where the objective  $\mathcal{L}$  is imposed. We do not alter the  $\mathcal{L}$  itself; instead, training relies on minimizing the contrastive loss  $\mathcal{L}$  between  $\pi(e_1|\omega_1)$  and  $\pi(e_2|\omega_2)$ . Thus,  $\pi$  learns to draw  $e_1$  and  $e_2$  together in its representation space *on condition of*  $\omega_1$  and  $\omega_2$ . We visualize the architecture of CASSLE in Figure 2.

We provide a rationale for why CASSLE preserves information about augmented features in the representation space. Since augmentation information vectors  $\omega$  do not carry any information about

<sup>3</sup>While contrastive objectives such as InfoNCE [64] regularize the representation using negative pairs, we omit them from our notation for the sake of brevity.

source images  $\mathbf{x}$ , their usefulness during pretraining could be explained only by using knowledge of transformations  $t_\omega$  that had been applied to  $\mathbf{x}$  to form views  $\mathbf{v}$ . However, for such knowledge to be acted upon, features affected by  $t_\omega$  must be preserved in the feature extractor representation  $f(\mathbf{v})$ .

Let us assume the opposite, that  $\omega$  is not useful for CASSLE to solve the task defined by  $\mathcal{L}$ . If this is the case, then for any  $\omega_3 \sim \Omega$  the following would hold:

$$p(\pi(\mathbf{e}_1|\omega_1)|\pi(\mathbf{e}_2|\omega_2)) = p(\pi(\mathbf{e}_1|\omega_1)|\pi(\mathbf{e}_2|\omega_3)). \quad (1)$$

$p(\pi(\mathbf{e}_1|\omega_1)|\pi(\mathbf{e}_2|\omega_2))$  can be understood as conditional probability that  $\pi(\mathbf{e}_1|\omega_1)$  is a representation of an image  $\mathbf{x}$  transformed by  $t_{\omega_1}$ , given the knowledge that  $\pi(\mathbf{e}_2|\omega_2)$  is a representation of  $\mathbf{x}$  transformed by  $t_{\omega_2}$ . Equation 1 implies that replacing the knowledge of  $t_{\omega_2}$  with any other randomly sampled  $t_{\omega_3}$  does not affect the inference process of CASSLE.

To demonstrate that this is not the case, we measure the similarity of representations of 5000 positive image pairs from the ImageNet-100 test set, where one representation is always constructed using true information about applied augmentations, and the second is constructed using either true or randomly sampled augmentation information. It is evident from Figure 3 that the similarity of embeddings decreases when false augmentation parameters ( $\omega_3$  instead of  $\omega_2$ ) are supplied to the projector, i.e.:

$$\mathbb{E}_{x \sim \mathbb{X}, \{\omega_1, \omega_2, \omega_3\} \sim \Omega} [ \text{sim}(\pi(\mathbf{e}_1|\omega_1), \pi(\mathbf{e}_2|\omega_2)) - \text{sim}(\pi(\mathbf{e}_1|\omega_1), \pi(\mathbf{e}_2|\omega_3)) ] > 0. \quad (2)$$

Recall that in contrastive SSL, the similarity of embeddings corresponds to their probability density. This is because the InfoNCE loss is formulated as cross-entropy, where the activation function is defined as similarity between respective image embeddings, and class labels are replaced with the indices of corresponding positive embedding pairs [64, 32, 15]. Hence, minimizing  $\mathcal{L}$  leads to:

$$\text{sim}(\pi(\mathbf{e}_1|\omega_1), \pi(\mathbf{e}_2|\omega_2)) \propto \frac{p(\pi(\mathbf{e}_1|\omega_1)|\pi(\mathbf{e}_2|\omega_2))}{p(\pi(\mathbf{e}_1|\omega_1))}. \quad (3)$$

It follows from 2 that, in practice

$$\mathbb{E}_{x \sim \mathbb{X}, \{\omega_1, \omega_2, \omega_3\} \sim \Omega} \left[ \frac{p(\pi(\mathbf{e}_1|\omega_1)|\pi(\mathbf{e}_2|\omega_2)) - p(\pi(\mathbf{e}_1|\omega_1)|\pi(\mathbf{e}_2|\omega_3))}{p(\pi(\mathbf{e}_1|\omega_1))} \right] > 0 \quad (4)$$

and, since  $p(\pi(\mathbf{e}_1|\omega_1)) > 0$ ,

$$\mathbb{E}_{x \sim \mathbb{X}, \{\omega_1, \omega_2, \omega_3\} \sim \Omega} [p(\pi(\mathbf{e}_1|\omega_1)|\pi(\mathbf{e}_2|\omega_2)) - p(\pi(\mathbf{e}_1|\omega_1)|\pi(\mathbf{e}_2|\omega_3))] > 0. \quad (5)$$

Moreover, we measure whether  $p(\pi(\mathbf{e}_1|\omega_1)|\pi(\mathbf{e}_2|\omega_2)) > p(\pi(\mathbf{e}_1|\omega_1)|\pi(\mathbf{e}_2|\omega_3))$  for each of the considered image view pairs and find it to be true in 92% of the considered cases.

In CASSLE, *the conditional probability of matching a positive pair of image representations increases when the correct augmentation information is known*, which implies that information pertaining to augmented features is indeed preserved in the representation of its feature extractor.

CASSLE can be applied to a variety of joint-embedding SSL methods, as the only practical modification it makes is changing the projector network to utilize the additional input  $\omega$ , describing the augmentations. We do not modify any other aspects of the self-supervised approaches, such as objective functions, which is appealing from a practical perspective. Last but not least, the architecture of the feature extractor in CASSLE is not affected by the introduced augmentation conditioning, as we only modify the input to the projector, which is discarded after the pretraining. Just like in vanilla SSL techniques, the feature extractor can be directly used in downstream tasks.

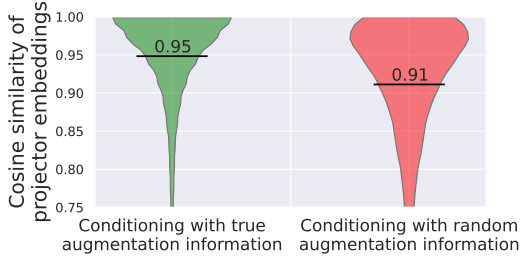


Figure 3: Similarities of CASSLE projector representations when conditioned with augmentation information from either their respective images (green), or randomly sampled (red). Solid lines denote the mean values of similarities. Conditioning the CASSLE projector with wrong augmentation information decreases its ability to draw image pairs together, indicating that it indeed relies on augmentation information to perform its task.

### 3.3 Practical implementation of the conditioning mechanism

In this work, we focus on a set of augmentations used commonly in the literature [15, 17, 18], listed below along with descriptions of their respective parameters  $\omega^{aug}$ :

- **random cropping** –  $\omega^c \in [0, 1]^4$  describes the normalized coordinates of cropped image center and cropping sizes.
- **color jittering** –  $\omega^j \in [0, 1]^4$  describes the normalized intensities of brightness, contrast, saturation, and hue adjustment.
- **Gaussian blurring** –  $\omega^b \in [0, 1]$  is the standard deviation of the Gaussian filter used during the blurring operation.
- **random horizontal flipping** –  $\omega^f \in \{0, 1\}$  indicates whether the image has been flipped.
- **random grayscaling** –  $\omega^g \in \{0, 1\}$  indicates whether the image has been reduced to grayscale.

To enhance the projector’s awareness of the color changes in the augmented images, we additionally enrich  $\omega$  with information about **color difference** –  $\omega^d \in [0, 1]^3$ , which is computed as the difference between the mean values of color channels of the image before and after the color jittering operation. We empirically demonstrate that inclusion of  $\omega^d$  in  $\omega$  improves the performance of CASSLE (see Section 4.3).

We construct augmentation information  $\omega \in \Omega$  by concatenating vectors  $\omega^{aug}$  describing the parameters of each augmentation type [40]. We consider four methods of injecting  $\omega$  into  $\pi$ : joining  $\omega$  and  $\mathbf{e}$  through (i) concatenation, modulating  $\mathbf{e}$  with  $\omega$  through element-wise (ii) addition or (iii) multiplication, or (iv) using  $\omega$  as an input to a hypernetwork [31] which generates the parameters of  $\pi$ . Apart from concatenation, all of those methods require transforming  $\omega$  into *augmentation embeddings*  $\mathbf{g} \in \mathcal{G}$  of shapes required by the conditioning operation. For example, when modulating  $\mathbf{e}$  with  $\mathbf{g}$ , dimensions of  $\mathbf{e}$  and  $\mathbf{g}$  must be equal. For this purpose, we precede the projector with additional *Augmentation encoder*  $\gamma : \Omega \rightarrow \mathcal{G}$ . For the architecture of  $\gamma$  we choose the Multilayer Perceptron. An additional advantage of  $\gamma$  is that it allows for learning a representation of  $\omega$  which is more expressive for processing by  $\pi$ , which is typically a shallow network. In practice, we find that conditioning  $\pi$  through the concatenation of  $\mathbf{e}$  and  $\mathbf{g}$  yields the best-performing representation (see Section 4.3).

## 4 Experiments

In Section 4.1, we evaluate CASSLE’s performance on downstream tasks such as classification, regression, and object detection<sup>4</sup>. In Section 4.2, we analyze the representations formed by CASSLE. Finally, we discuss the choice of hyperparameters of CASSLE in Section 4.3. In all experiments, unless specified otherwise, we utilize the ResNet-50 architecture [33] and conduct the self-supervised pretraining on ImageNet-100 - a 100-class subset of the ILSVRC dataset [58] used commonly in the literature [62, 69, 40, 14]. We use the standard set of augmentations including horizontal flipping, random cropping, grayscaling, color jittering and Gaussian blurring [32, 40, 30]. For consistency in terms of hyperparameters, we follow [40] for MoCo-v2, and [14] for SimCLR. We include comparisons on other SSL frameworks [32, 30, 18, 72], extended analysis of trained representations, as well as additional details of training and evaluation, in the supplementary material.

### 4.1 Evaluation on downstream tasks

We begin the experimental analysis by addressing the most fundamental question – how does CASSLE impact the ability of models to generalize? In order to answer it, we evaluate models pretrained via CASSLE and other self-supervised techniques on a variety of downstream visual tasks, such as classification, regression, and object detection.

---

<sup>4</sup>We compare CASSLE to a number of recently proposed methods and report their performance from the literature [69, 40, 14], given that the code for [69] and [14] was not made available at the time of writing. As for the results of baseline SSL models and AugSelf [40], we report their results from the literature except when our runs of those methods yielded results different by at least 2 pp. We mark such cases with †.

Table 1: Linear evaluation on downstream classification and regression tasks. CASSLE consistently improves representations formed by vanilla SSL approaches and performs better or comparably to other techniques of increasing sensitivity to augmentations [69, 40, 14].

Method	C10	C100	Food	MIT	Pets	Flowers	Caltech	Cars	FGVCA	DTD	SUN	CUB	300W
<i>SimCLR</i> [15]													
Vanilla	84.41 <sup>†</sup>	61.40	57.48 <sup>†</sup>	63.10 <sup>†</sup>	71.60 <sup>†</sup>	83.37 <sup>†</sup>	<b>79.67<sup>†</sup></b>	35.14 <sup>†</sup>	40.03 <sup>†</sup>	64.90	46.92 <sup>†</sup>	30.98 <sup>†</sup>	88.59 <sup>†</sup>
AugSelf [40] <sup>†</sup>	84.45	62.67	59.96	63.21	70.61	<b>85.77</b>	77.78	37.38	42.86	65.53	<b>49.18</b>	34.24	88.27
AI [14]	83.90	63.10	–	–	69.50	68.30	74.20	–	–	53.70	–	<b>38.60</b>	88.00
<b>CASSLE</b>	<b>86.31</b>	<b>64.36</b>	<b>60.67</b>	<b>63.96</b>	<b>72.33</b>	85.22	79.62	<b>39.86</b>	<b>43.10</b>	<b>65.96</b>	48.91	33.21	<b>88.88</b>
<i>MoCo-v2</i> [32, 17]													
Vanilla	84.60	61.60	59.67	61.64	70.08	82.43	77.25	33.86	41.21	64.47	46.50	32.20	88.77 <sup>†</sup>
AugSelf [40]	85.26	63.90	60.78	63.36	73.46	85.70	78.93	37.35	39.47	66.22	48.52	37.00	89.49 <sup>†</sup>
AI [14]	81.30	64.60	–	–	<b>74.00</b>	81.30	78.90	–	–	<b>68.80</b>	–	<b>41.40</b>	<b>90.00</b>
LooC [69]	–	–	–	–	–	–	–	–	–	–	39.60	–	–
IFM [57] <sup>†</sup>	83.36	60.22	59.86	60.60	72.99	85.73	78.77	36.54	41.05	62.34	47.48	35.90	88.92
<b>CASSLE</b>	<b>86.32</b>	<b>65.29</b>	<b>61.93</b>	<b>63.86</b>	72.86	<b>86.51</b>	<b>79.63</b>	<b>38.82</b>	<b>42.03</b>	66.54	<b>49.25</b>	36.22	88.93
<i>MoCo-v3</i> [19] with ViT-Small [23] pretrained on the full ImageNet dataset.													
Vanilla <sup>†</sup>	83.17	62.40	56.15	53.28	62.29	81.48	69.63	28.63	32.84	57.18	42.16	35.00	87.42
AugSelf [40] <sup>†</sup>	84.25	64.12	<b>58.28</b>	<b>56.12</b>	<b>63.93</b>	<b>83.13</b>	72.45	29.64	32.54	<b>60.27</b>	43.22	<b>37.16</b>	87.85
<b>CASSLE</b>	<b>85.13</b>	<b>64.67</b>	57.30	55.90	63.88	82.42	<b>73.53</b>	<b>30.92</b>	<b>35.91</b>	58.24	<b>43.37</b>	36.09	<b>88.53</b>

**Linear evaluation** We evaluate the performance of pretrained networks on the downstream tasks of classification on a wide array of datasets: CIFAR10/100 (C10/100) [39], Food101 (Food) [10], MIT67 (MIT) [54], Oxford-IIIT Pets (Pets) [51], Oxford Flowers-102 (Flowers) [47], Caltech101 (Caltech) [26], Stanford Cars (Cars) [38], FGVC-Aircraft (FGVCA) [43], Describable Textures (DTD) [20], SUN-397 (SUN) [68], as well as regression on the 300 Faces In-the-Wild (300W) dataset [59]. We follow the linear evaluation protocol [37, 15, 40], described in detail in the supplementary material. We evaluate multiple self-supervised methods extended with CASSLE, as well as other recently proposed extensions which increase sensitivity to augmentations [40, 69, 14] or prevent feature suppression in SSL [57]. We report the full results in Tables 1 and 7. We find that in the vast majority of cases, CASSLE improves the performance of vanilla joint-embedding methods, as well as other other SSL extensions that foster augmentation sensitivity [40, 14].

**Object detection** We next evaluate the pretrained networks on a more challenging task of object detection on the VOC 2007 dataset [25]. We follow the training scheme of [32, 17], except that we only train the object detector modules and keep the feature extractor parameters fixed during training for detection to better compare the pretrained representations. We report the Average Precision (AP) [42] of models pretrained through MoCo-v2 and SimCLR [15] with AugSelf [40] and CASSLE extensions in Table 2. The compared approaches yield similar results, with CASSLE representation slightly surpassing the vanilla methods and AugSelf.

Table 2: Average Precision of object detection on VOC dataset [25, 42]. CASSLE extension of MoCo-v2 and SimCLR outperforms the vanilla approaches and AugSelf extension by a small margin.

Method	<i>MoCo-v2</i>	<i>SimCLR</i>
Vanilla	45.12	44.74
AugSelf [40]	45.20	44.50
<b>CASSLE</b>	<b>45.90</b>	<b>45.60</b>

## 4.2 Analysis of representations formed by CASSLE

We investigate the awareness of augmentation-induced data perturbations in the intermediate and final representations of pretrained networks. As a proxy metric for measuring this, we choose the InfoNCE loss [64, 15]. The value of InfoNCE is high if embeddings of pairs of augmented images are less similar to one another than to embeddings of unrelated images, and low if positive pairs of embeddings are on average separated correctly, and thus, the given representation is invariant to augmentations. We report the mean InfoNCE loss values under different augmentation types at subsequent stages of ResNet-50 and projectors of MoCo-v2, AugSelf [40] and CASSLE in Figure 4.

In all networks, the augmentation awareness decreases gradually throughout the feature extractor and projector stages. In CASSLE, we observe a much softer decline in the feature extractor stages

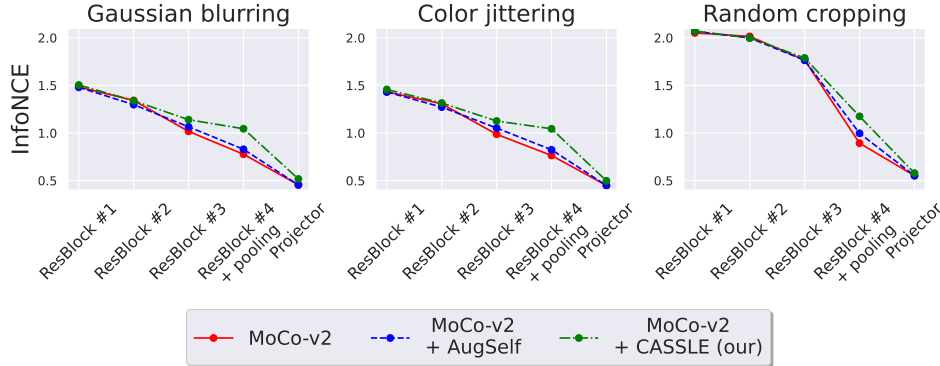


Figure 4: A comparison of InfoNCE loss measured on different kinds of augmentations at subsequent stages of the ResNet-50 and projectors pretrained by vanilla, AugSelf [40] and CASSLE variants of MoCo-v2. Feature extractor representation of CASSLE yields higher InfoNCE values which suggests that it is more susceptible to augmentations.

and a sharper one in the projector. Representations of CASSLE feature extractor are on average more difficult to match together than those of vanilla MoCo-v2 and AugSelf [40]. This implies that the CASSLE feature extractor is indeed more sensitive to augmentations than its counterparts. On the other hand, representations of all projectors, including CASSLE, are similarly separable. This suggests that the conditioning mechanism helps CASSLE projector to better amortize the augmentation-induced differences between the feature extractor embeddings.

The above observations indicate that in the vanilla and (to a slightly lesser extent) AugSelf approaches, both the projector and the intermediate representations are enforced to be augmentation-invariant. On the other hand, in CASSLE, the task of augmentation invariance is solved to a larger degree by the projector, and to a smaller degree by the feature extractor, allowing it to be more augmentation-aware. As shown in Section 4.1, this sensitivity does not prevent the CASSLE feature extractor from achieving similar or better performance than its counterparts when transferred to downstream tasks.

### 4.3 Ablation Study

In this section, we examine the impact of different hyperparameters of CASSLE. We compare different variants of MoCo-v2+CASSLE on the same classification and regression tasks as in Section 4.1. We rank the models from best to worst performance on each task and report the average ranks in Table 3. We provide the detailed results in the supplementary material.

**Augmentation information contents** – We compare conditioning the projector with different subsets of augmentation information. The average best representation is trained with conditioning on all possible augmentation information. Moreover, using the additional **color difference** ( $\omega^d$ ) information additionally improves the results, indicating that it is indeed useful to consider not only augmentation parameters but also information about its effects.

**Impact of utilizing color difference information** – We verify that the improved performance of CASSLE does not stem solely from using augmentation information that has not been considered in prior works. We compare a variant of AugSelf which learns to predict color difference values ( $\omega^d$ ) in addition to augmentation information used by [40], i.e. cropping ( $\omega^c$ ) and color jittering ( $\omega^j$ ), as well as a variant of CASSLE conditioned on all augmentation information *except*  $\omega^d$  (i.e.  $\omega^{\{c,j,b,f,g\}}$ ). We find that while including  $\omega^d$  improves the performance of AugSelf and CASSLE, both variants of CASSLE achieve better results than both variants of AugSelf.

**Method of conditioning the projector** – We compare conditioning the projector through (i) concatenation, element-wise (ii) addition or (iii) multiplication, or (iv) using  $\pi$  as an input to a hypernetwork [31] which generates the parameters of  $\pi$ . Conditioning through **concatenation** and **addition** yields on average the strongest performance on downstream tasks. We choose to utilize the **concatenation** method in our experiments, as it requires a slightly smaller Augmentation encoder.



Table 3: Ablation study of CASSLE parameters. CASSLE performs best when conditioned on all available augmentation information, by concatenating or adding the augmentation and image embeddings.

Augmentation information	Average rank ↓	Method	Average rank ↓	Conditioning method	Average rank ↓	Number of layers	Average rank ↓
$\omega^{\{c\}}$	4.54					0	3.38
$\omega^{\{c,j\}}$	4.54	A – $\omega^{\{c,j\}}$	3.07	Concatenation	<b>1.92</b>	2	3.08
$\omega^{\{c,j,d\}}$	3.08	C – $\omega^{\{c,j,b,f,g\}}$	2.64	Addition	<b>1.92</b>	4	2.38
$\omega^{\{c,j,b,f\}}$	2.85	A – $\omega^{\{c,j,d\}}$	2.71	Multiplication	2.69	6	<b>2.15</b>
$\omega^{\{c,j,b,f,g\}}$	3.54	C – $\omega^{\{c,j,b,f,g,d\}}$	<b>1.57</b>	Hypernetwork	3.46	8	4.00
$\omega^{\{c,j,b,f,g,d\}}$	<b>2.54</b>						

(a) Augmentation information used for conditioning

(b) Impact of including color difference information ( $\omega^d$ ) on AugSelf and CASSLE

(c) Method of conditioning the projector

(d) Augmentation encoder depth (0 denotes concatenating raw  $\omega$  to e)

**Size of the Augmentation encoder** – While CASSLE is robust to the size of the  $\gamma$  MLP, using the depth and hidden size of 6 and 64, respectively, yields the strongest downstream performance. In particular, the variant of CASSLE that utilizes the Augmentation encoder performs better than the variant that concatenates e to raw augmentation embeddings  $\omega$ . Given such an architecture of the Augmentation encoder, our computation overhead is negligible as we increase the overall number of parameters by around 0.1%. We refer to the supplementary material for the detailed ablation of the Augmentation encoder’s hidden size.

## 5 Conclusion

In this paper, we propose a novel method for augmentation-aware self-supervised learning that retains information about data augmentations in the representation space. To accomplish this, we introduce the concept of the conditioned projector, which receives augmentation information while processing the representation vector. Our solution necessitates only small architectural changes and no additional auxiliary loss components. Therefore, the training concentrates on contrastive loss, which enhances overall performance.

We compare our solution with existing augmentation-aware SSL methods and demonstrate its superior performance on downstream tasks, particularly when augmentation invariance leads to the loss of vital information. Moreover, we show that it obtains representations more sensitive to augmentations than the baseline methods.

Overall, our method offers a straightforward and efficient approach to retaining information about data augmentations in the representation space. It can be directly applied to SSL methods, contributing to the further advancement of augmentation-aware self-supervised learning.

**Reproducibility statement** The codebase for CASSLE is available at <https://github.com/gmum/CASSLE>. We detail the hyperparameters for training runs in the supplementary material. All datasets used for training and evaluation are publicly available.

## References

- [1] Kumar Krishna Agrawal, Arnab Kumar Mondal, Arna Ghosh, and Blake Aaron Richards.  $\alpha$ -req: Assessing representation quality in self-supervised learning by measuring eigenspectrum decay. In Alice H. Oh, Alekh Agarwal, Danielle Belgrave, and Kyunghyun Cho, editors, *Advances in Neural Information Processing Systems*, 2022.
- [2] Saleh Albelwi. Survey on self-supervised learning: Auxiliary pretext tasks and contrastive learning methods in imaging. *Entropy*, 24(4), 2022.
- [3] Haoping Bai, Meng Cao, Ping Huang, and Jiulong Shan. Self-supervised semi-supervised learning for data labeling and quality evaluation. In *NeurIPS Workshop*, 2021.
- [4] Randall Balestriero, Mark Ibrahim, Vlad Sobal, Ari Morcos, Shashank Shekhar, Tom Goldstein, Florian Bordes, Adrien Bardes, Gregoire Mialon, Yuandong Tian, Avi Schwarzschild, Andrew Gordon Wilson,

- Jonas Geiping, Quentin Garrido, Pierre Fernandez, Amir Bar, Hamed Pirsiavash, Yann LeCun, and Micah Goldblum. A cookbook of self-supervised learning, 2023.
- [5] Adrien Bardes, Jean Ponce, and Yann LeCun. VICReg: Variance-invariance-covariance regularization for self-supervised learning. In *International Conference on Learning Representations*, 2022.
- [6] Suzanna Becker and Geoffrey Hinton. Self-organizing neural network that discovers surfaces in random-dot stereograms. *Nature*, 355:161–3, 02 1992.
- [7] Javad Zolfaghari Bengar, Joost van de Weijer, Bartłomiej Twardowski, and Bogdan Raducanu. Reducing label effort: Self-supervised meets active learning. In *Proceedings of the IEEE/CVF International Conference on Computer Vision (ICCV) Workshops*, pages 1631–1639, October 2021.
- [8] Sangnie Bhardwaj, Willie McClinton, Tongzhou Wang, Guillaume Lajoie, Chen Sun, Phillip Isola, and Dilip Krishnan. Steerable equivariant representation learning, 2023.
- [9] Florian Bordes, Randall Balestriero, Quentin Garrido, Adrien Bardes, and Pascal Vincent. Guillotine regularization: Why removing layers is needed to improve generalization in self-supervised learning. *Transactions on Machine Learning Research*, 2023.
- [10] Lukas Bossard, Matthieu Guillaumin, and Luc Van Gool. Food-101 – mining discriminative components with random forests. In *European Conference on Computer Vision*, 2014.
- [11] Tom Brown, Benjamin Mann, Nick Ryder, Melanie Subbiah, Jared D Kaplan, Prafulla Dhariwal, Arvind Neelakantan, Pranav Shyam, Girish Sastry, Amanda Askell, et al. Language models are few-shot learners. volume 33, pages 1877–1901, 2020.
- [12] Mathilde Caron, Ishan Misra, Julien Mairal, Priya Goyal, Piotr Bojanowski, and Armand Joulin. Unsupervised learning of visual features by contrasting cluster assignments. In H. Larochelle, M. Ranzato, R. Hadsell, M.F. Balcan, and H. Lin, editors, *Advances in Neural Information Processing Systems*, volume 33, pages 9912–9924. Curran Associates, Inc., 2020.
- [13] Mathilde Caron, Hugo Touvron, Ishan Misra, Hervé Jégou, Julien Mairal, Piotr Bojanowski, and Armand Joulin. Emerging properties in self-supervised vision transformers. In *Proceedings of the International Conference on Computer Vision (ICCV)*, 2021.
- [14] Ruchika Chavhan, Jan Stuehmer, Calum Heggan, Mehrdad Yaghoobi, and Timothy Hospedales. Amortised invariance learning for contrastive self-supervision. In *The Eleventh International Conference on Learning Representations*, 2023.
- [15] Ting Chen, Simon Kornblith, Mohammad Norouzi, and Geoffrey Hinton. A simple framework for contrastive learning of visual representations. In Hal Daumé III and Aarti Singh, editors, *Proceedings of the 37th International Conference on Machine Learning*, volume 119 of *Proceedings of Machine Learning Research*, pages 1597–1607. PMLR, 13–18 Jul 2020.
- [16] Ting Chen, Calvin Luo, and Lala Li. Intriguing properties of contrastive losses. In A. Beygelzimer, Y. Dauphin, P. Liang, and J. Wortman Vaughan, editors, *Advances in Neural Information Processing Systems*, 2021.
- [17] Xinlei Chen, Haoqi Fan, Ross Girshick, and Kaiming He. Improved baselines with momentum contrastive learning, 2020.
- [18] Xinlei Chen and Kaiming He. Exploring simple siamese representation learning. In *Proceedings of the IEEE/CVF Conference on Computer Vision and Pattern Recognition (CVPR)*, pages 15750–15758, June 2021.
- [19] Xinlei Chen, Saining Xie, and Kaiming He. An empirical study of training self-supervised vision transformers. In *Proceedings of the IEEE/CVF International Conference on Computer Vision (ICCV)*, pages 9640–9649, October 2021.
- [20] M. Cimpoi, S. Maji, I. Kokkinos, S. Mohamed, , and A. Vedaldi. Describing textures in the wild. In *Proceedings of the IEEE Conf. on Computer Vision and Pattern Recognition (CVPR)*, 2014.
- [21] Jacob Devlin, Ming-Wei Chang, Kenton Lee, and Kristina Toutanova. BERT: Pre-training of deep bidirectional transformers for language understanding, June 2019.
- [22] Carl Doersch, Abhinav Gupta, and Alexei A. Efros. Unsupervised visual representation learning by context prediction. In *Proceedings of the IEEE International Conference on Computer Vision (ICCV)*, December 2015.
- [23] Alexey Dosovitskiy, Lucas Beyer, Alexander Kolesnikov, Dirk Weissenborn, Xiaohua Zhai, Thomas Unterthiner, Mostafa Dehghani, Matthias Minderer, Georg Heigold, Sylvain Gelly, Jakob Uszkoreit, and Neil Houlsby. An image is worth 16x16 words: Transformers for image recognition at scale. In *International Conference on Learning Representations*, 2021.
- [24] Linus Ericsson, Henry Gouk, and Timothy M. Hospedales. Why do self-supervised models transfer? investigating the impact of invariance on downstream tasks, 2022.

- [25] M. Everingham, L. Van Gool, C. K. I. Williams, J. Winn, and A. Zisserman. The PASCAL Visual Object Classes Challenge 2007 (VOC2007) Results. <http://www.pascal-network.org/challenges/VOC/voc2007/workshop/index.html>.
- [26] Li Fei-Fei, R. Fergus, and P. Perona. One-shot learning of object categories. *IEEE Transactions on Pattern Analysis and Machine Intelligence*, 28(4):594–611, 2006.
- [27] Quentin Garrido, Laurent Najman, and Yann Lecun. Self-supervised learning of split invariant equivariant representations. In Andreas Krause, Emma Brunskill, Kyunghyun Cho, Barbara Engelhardt, Sivan Sabato, and Jonathan Scarlett, editors, *Proceedings of the 40th International Conference on Machine Learning*, volume 202 of *Proceedings of Machine Learning Research*, pages 10975–10996. PMLR, 23–29 Jul 2023.
- [28] Spyros Gidaris, Praveer Singh, and Nikos Komodakis. Unsupervised representation learning by predicting image rotations. In *International Conference on Learning Representations*, 2018.
- [29] Ian Goodfellow, Yoshua Bengio, and Aaron Courville. *Deep learning*. MIT press, 2016.
- [30] Jean-Bastien Grill, Florian Strub, Florent Altché, Corentin Tallec, Pierre Richemond, Elena Buchatskaya, Carl Doersch, Bernardo Avila Pires, Zhaohan Guo, Mohammad Gheshlaghi Azar, Bilal Piot, Koray Kavukcuoglu, Remi Munos, and Michal Valko. Bootstrap your own latent - a new approach to self-supervised learning. In H. Larochelle, M. Ranzato, R. Hadsell, M.F. Balcan, and H. Lin, editors, *Advances in Neural Information Processing Systems*, volume 33, pages 21271–21284. Curran Associates, Inc., 2020.
- [31] David Ha, Andrew M. Dai, and Quoc V. Le. Hypernetworks. In *International Conference on Learning Representations*, 2017.
- [32] Kaiming He, Haoqi Fan, Yuxin Wu, Saining Xie, and Ross Girshick. Momentum contrast for unsupervised visual representation learning. In *Proceedings of the IEEE/CVF Conference on Computer Vision and Pattern Recognition (CVPR)*, June 2020.
- [33] Kaiming He, Xiangyu Zhang, Shaoqing Ren, and Jian Sun. Deep residual learning for image recognition, June 2016.
- [34] Dan Hendrycks and Thomas Dietterich. Benchmarking neural network robustness to common corruptions and perturbations. In *International Conference on Learning Representations*, 2019.
- [35] Li Jing, Pascal Vincent, Yann LeCun, and Yuandong Tian. Understanding dimensional collapse in contrastive self-supervised learning. In *International Conference on Learning Representations*, 2022.
- [36] Tae Soo Kim, Geonwoon Jang, Sanghyup Lee, and Thijs Kooi. Did you get what you paid for? rethinking annotation cost of deep learning based computer aided detection in chest radiographs, 2022.
- [37] Simon Kornblith, Jonathon Shlens, and Quoc V. Le. Do better imagenet models transfer better?, June 2019.
- [38] Jonathan Krause, Michael Stark, Jia Deng, and Li Fei-Fei. 3d object representations for fine-grained categorization. In *4th International IEEE Workshop on 3D Representation and Recognition (3dRR-13)*, Sydney, Australia, 2013.
- [39] Alex Krizhevsky. Learning multiple layers of features from tiny images. 2009.
- [40] Hankook Lee, Kibok Lee, Kimin Lee, Honglak Lee, and Jinwoo Shin. Improving transferability of representations via augmentation-aware self-supervision. 34:17710–17722, 2021.
- [41] Xuhong LI, Yves Grandvalet, and Franck Davoine. Explicit inductive bias for transfer learning with convolutional networks. In Jennifer Dy and Andreas Krause, editors, *Proceedings of the 35th International Conference on Machine Learning*, volume 80 of *Proceedings of Machine Learning Research*, pages 2825–2834. PMLR, 10–15 Jul 2018.
- [42] Tsung-Yi Lin, Michael Maire, Serge J. Belongie, Lubomir D. Bourdev, Ross B. Girshick, James Hays, Pietro Perona, Deva Ramanan, Piotr Dollár, and C. Lawrence Zitnick. Microsoft COCO: common objects in context. *CoRR*, abs/1405.0312, 2014.
- [43] Subhransu Maji, Esa Rahtu, Juho Kannala, Matthew Blaschko, and Andrea Vedaldi. Fine-grained visual classification of aircraft, 2013.
- [44] Grégoire Mialon, Randall Balestriero, and Yann LeCun. Variance covariance regularization enforces pairwise independence in self-supervised representations, 2023.
- [45] Volodymyr Mnih, Koray Kavukcuoglu, David Silver, Andrei A Rusu, Joel Veness, Marc G Bellemare, Alex Graves, Martin Riedmiller, Andreas K Fidjeland, Georg Ostrovski, et al. Human-level control through deep reinforcement learning. *nature*, 518(7540):529–533, 2015.
- [46] Sharada P. Mohanty, David P. Hughes, and Marcel Salathé. Using deep learning for image-based plant disease detection, 2016.
- [47] Maria-Elena Nilsback and Andrew Zisserman. Automated flower classification over a large number of classes. In *Indian Conference on Computer Vision, Graphics and Image Processing*, Dec 2008.

- [48] Mehdi Noroozi and Paolo Favaro. Unsupervised learning of visual representations by solving jigsaw puzzles. In Bastian Leibe, Jiri Matas, Nicu Sebe, and Max Welling, editors, *Computer Vision – ECCV 2016*, pages 69–84, Cham, 2016. Springer International Publishing.
- [49] Maxime Oquab, Timothée Darcet, Théo Moutakanni, Huy Vo, Marc Szafraniec, Vasil Khalidov, Pierre Fernandez, Daniel Haziza, Francisco Massa, Alaaeldin El-Nouby, Mahmoud Assran, Nicolas Ballas, Wojciech Galuba, Russell Howes, Po-Yao Huang, Shang-Wen Li, Ishan Misra, Michael Rabbat, Vasu Sharma, Gabriel Synnaeve, Hu Xu, Hervé Jegou, Julien Mairal, Patrick Labatut, Armand Joulin, and Piotr Bojanowski. Dinov2: Learning robust visual features without supervision, 2023.
- [50] Boris Oreshkin, Pau Rodríguez López, and Alexandre Lacoste. Tadam: Task dependent adaptive metric for improved few-shot learning, 2018.
- [51] Omkar M. Parkhi, Andrea Vedaldi, Andrew Zisserman, and C. V. Jawahar. Cats and dogs. In *IEEE Conference on Computer Vision and Pattern Recognition*, 2012.
- [52] Adam Paszke, Sam Gross, Francisco Massa, Adam Lerer, James Bradbury, Gregory Chanan, Trevor Killeen, Zeming Lin, Natalia Gimelshein, Luca Antiga, Alban Desmaison, Andreas Kopf, Edward Yang, Zachary DeVito, Martin Raison, Alykhan Tejani, Sasank Chilamkurthy, Benoit Steiner, Lu Fang, Junjie Bai, and Soumith Chintala. Pytorch: An imperative style, high-performance deep learning library. In *Advances in Neural Information Processing Systems 32*, pages 8024–8035. Curran Associates, Inc., 2019.
- [53] F. Pedregosa, G. Varoquaux, A. Gramfort, V. Michel, B. Thirion, O. Grisel, M. Blondel, P. Prettenhofer, R. Weiss, V. Dubourg, J. Vanderplas, A. Passos, D. Cournapeau, M. Brucher, M. Perrot, and E. Duchesnay. Scikit-learn: Machine learning in Python. *Journal of Machine Learning Research*, 12:2825–2830, 2011.
- [54] Ariadna Quattoni and Antonio Torralba. Recognizing indoor scenes. In *2009 IEEE Conference on Computer Vision and Pattern Recognition*, pages 413–420, 2009.
- [55] Aniruddh Raghu, Jonathan Lorraine, Simon Kornblith, Matthew McDermott, and David K Duvenaud. Meta-learning to improve pre-training. In M. Ranzato, A. Beygelzimer, Y. Dauphin, P.S. Liang, and J. Wortman Vaughan, editors, *Advances in Neural Information Processing Systems*, volume 34, pages 23231–23244. Curran Associates, Inc., 2021.
- [56] Shaoqing Ren, Kaiming He, Ross Girshick, and Jian Sun. Faster r-cnn: Towards real-time object detection with region proposal networks. In C. Cortes, N. Lawrence, D. Lee, M. Sugiyama, and R. Garnett, editors, *Advances in Neural Information Processing Systems*, volume 28. Curran Associates, Inc., 2015.
- [57] Joshua Robinson, Li Sun, Ke Yu, Kayhan Batmanghelich, Stefanie Jegelka, and Suvrit Sra. Can contrastive learning avoid shortcut solutions? In M. Ranzato, A. Beygelzimer, Y. Dauphin, P.S. Liang, and J. Wortman Vaughan, editors, *Advances in Neural Information Processing Systems*, volume 34, pages 4974–4986. Curran Associates, Inc., 2021.
- [58] Olga Russakovsky, Jia Deng, Hao Su, Jonathan Krause, Sanjeev Satheesh, Sean Ma, Zhiheng Huang, Andrej Karpathy, Aditya Khosla, Michael Bernstein, Alexander Berg, and Li Fei-Fei. Imagenet large scale visual recognition challenge, 09 2014.
- [59] C. Sagonas, E. Antonakos, Tzimiropoulos G, S. Zafeiriou, and M. Pantic. 300 faces in-the-wild challenge: Database and results. In *Image and Vision Computing (IMAVIS), Special Issue on Facial Landmark Localisation*, 2016.
- [60] Madeline C. Schiappa, Yogesh S. Rawat, and Mubarak Shah. Self-supervised learning for videos: A survey. *ACM Computing Surveys*, dec 2022.
- [61] Yisheng Song, Ting Wang, Puyu Cai, Subrota K. Mondal, and Jyoti Prakash Sahoo. A comprehensive survey of few-shot learning: Evolution, applications, challenges, and opportunities. volume 55, New York, NY, USA, jul 2023. Association for Computing Machinery.
- [62] Yonglong Tian, Chen Sun, Ben Poole, Dilip Krishnan, Cordelia Schmid, and Phillip Isola. What makes for good views for contrastive learning? 33:6827–6839, 2020.
- [63] Yuandong Tian. Understanding deep contrastive learning via coordinate-wise optimization. In Alice H. Oh, Alekh Agarwal, Danielle Belgrave, and Kyunghyun Cho, editors, *Advances in Neural Information Processing Systems*, 2022.
- [64] Aaron van den Oord, Yazhe Li, and Oriol Vinyals. Representation learning with contrastive predictive coding, 2019.
- [65] Diane Wagner, Fabio Ferreira, Danny Stoll, Robin Tibor Schirrmeyer, Samuel Müller, and Frank Hutter. On the importance of hyperparameters and data augmentation for self-supervised learning. In *First Workshop on Pre-training: Perspectives, Pitfalls, and Paths Forward at ICML 2022*, 2022.
- [66] C. Wah, S. Branson, P. Welinder, P. Perona, and S. Belongie. The Caltech-UCSD Birds-200-2011 Dataset. Technical Report CNS-TR-2011-001, California Institute of Technology, 2011.

- [67] Kristoffer Wickstrøm, Michael Kampffmeyer, Karl Øyvind Mikalsen, and Robert Jenssen. Mixing up contrastive learning: Self-supervised representation learning for time series. *Pattern Recognition Letters*, 155:54–61, mar 2022.
- [68] J. Xiao, J. Hays, K. A. Ehinger, A. Oliva, and A. Torralba. Sun database: Large-scale scene recognition from abbey to zoo. In *2010 IEEE Computer Society Conference on Computer Vision and Pattern Recognition*, pages 3485–3492, June 2010.
- [69] Tete Xiao, Xiaolong Wang, Alexei A Efros, and Trevor Darrell. What should not be contrastive in contrastive learning. In *International Conference on Learning Representations*, 2021.
- [70] Yuyang Xie, Jianhong Wen, Kin Wai Lau, Yasar Abbas Ur Rehman, and Jiajun Shen. What should be equivariant in self-supervised learning. In *Proceedings of the IEEE/CVF Conference on Computer Vision and Pattern Recognition (CVPR) Workshops*, pages 4111–4120, June 2022.
- [71] Jason Yosinski, Jeff Clune, Yoshua Bengio, and Hod Lipson. How transferable are features in deep neural networks? In Z. Ghahramani, M. Welling, C. Cortes, N. Lawrence, and K.Q. Weinberger, editors, *Advances in Neural Information Processing Systems*, volume 27. Curran Associates, Inc., 2014.
- [72] Jure Zbontar, Li Jing, Ishan Misra, Yann LeCun, and Stephane Deny. Barlow twins: Self-supervised learning via redundancy reduction. In Marina Meila and Tong Zhang, editors, *Proceedings of the 38th International Conference on Machine Learning*, volume 139 of *Proceedings of Machine Learning Research*, pages 12310–12320. PMLR, 18–24 Jul 2021.
- [73] Liheng Zhang, Guo-Jun Qi, Liqiang Wang, and Jiebo Luo. Aet vs. aed: Unsupervised representation learning by auto-encoding transformations rather than data. In *Proceedings of the IEEE/CVF Conference on Computer Vision and Pattern Recognition (CVPR)*, June 2019.
- [74] Richard Zhang, Phillip Isola, and Alexei A. Efros. Colorful image colorization. In Bastian Leibe, Jiri Matas, Nicu Sebe, and Max Welling, editors, *Computer Vision – ECCV 2016*, pages 649–666, Cham, 2016. Springer International Publishing.
- [75] Simone Zini, Alex Gomez-Villa, Marco Buzzelli, Bartłomiej Twardowski, Andrew D. Bagdanov, and Joost van de weijer. Planckian jitter: countering the color-crippling effects of color jitter on self-supervised training. In *The Eleventh International Conference on Learning Representations*, 2023.

## A Pretraining details

### A.1 Datasets

We use ImageNet-100, a 100-class subset of ImageNet [58, 62], to pretrain the standard ResNet-50 [33] architecture of self-supervised methods: MoCo-v2 [17], SimCLR [15], Barlow Twins [72], and SimSiam [18], as well as for common in the literature on augmentation-aware self-supervised learning [62, 69, 40, 14]. For MoCo-v3 [19], we pretrain the ViT-Small [23] model on the full ImageNet dataset [58].

### A.2 Hyperparameters

We follow the pretraining procedures from corresponding papers, described in [40] for MoCo-v2 and SimSiam, [14] for SimCLR, [72] for Barlow Twins, and [19] for MoCo-v3. We train variants of all SSL approaches on 2 and 8 NVidia A100 GPUs, except for SimCLR and MoCo-v3 which use larger batch sizes and therefore require 8 such GPUs. Synchronized batch normalization is employed for distributed training [18]. In Table 4, we present the training hyperparameters which are not related specifically to CASSLE, but rather joint-embedding approaches in general [32, 17, 15, 72, 18, 19].

### A.3 Augmentations

For self-supervised pretraining, we use a set of augmentations adopted commonly in the literature [32, 15, 17, 18, 72, 40]. We denote them below:

- **random cropping** – We sample the cropping scale randomly from [0.2, 1.0]. Afterward, we resize the cropped images to the size of  $224 \times 224$ .
- **color jittering** – We apply this operation with a probability of 0.8. We sample the intensities of brightness, contrast, saturation, and hue and their maximal values are 0.4, 0.4, 0.4, and 0.1, respectively.

Table 4: Hyperparameters of self-supervised methods used with CASSLE

SSL method	Architecture	Number of epochs	Batch size	Weight decay	Learning rate		Training time
					Base	Schedule	
MoCo-v1 [17]	ResNet-50	500	256	$10^{-4}$	0.03	Cosine decay	32h
MoCo-v2 [17]	ResNet-50	500	256	$10^{-4}$	0.03	Cosine decay	34h
SimCLR [15]	ResNet-50	300	1024	$10^{-4}$	0.05	Cosine decay	10h
Barlow Twins [72]	ResNet-50	500	256	$10^{-4}$	0.05	Cosine decay with warmup	36h
SimSiam [18]	ResNet-50	500	256	$10^{-4}$	0.05	Cosine decay	40h
MoCo-v3 [19]	ViT-small	300	1024	0.1	$1.5 \cdot 10^{-4}$	Cosine decay with warmup	23h

SSL method	Projector				Predictor			
	Depth	Hidden size	Out size	Final BatchNorm	Depth	Hidden size	Out size	Final BatchNorm
MoCo-v2	2	2048	128	No				No
SimCLR	2	2048	128	No				No
Barlow Twins	3	8192	8192	Yes, without affine transform				No
SimSiam	3	2048	2048	Yes	2	512	2048	No
MoCo-v3	3	4096	256	Yes, without affine transform	2	4096	256	Yes, without affine transform

- **Gaussian blurring** – We apply this operation with a probability of 0.5. We sample the standard deviation from  $[0.1, 2.0]$  and set the kernel size to  $23 \times 23$ .
- **random horizontal flipping** – We apply this operation with a probability of 0.5.
- **random grayscaling** – We apply this operation with a probability of 0.2.

## B Evaluation protocol

### B.1 Datasets

We outline the datasets and their respective evaluation metrics used for downstream tasks that we evaluate CASSLE on in Table 5.

Table 5: Information about datasets and their metrics used for downstream evaluation of CASSLE.

Downstream task	Dataset	Metric
Linear evaluation	CIFAR10 [39]	Top-1 accuracy
	CIFAR100 [39]	Top-1 accuracy
	Food101 [10]	Top-1 accuracy
	MIT67 [54]	Top-1 accuracy
	Oxford-IIIT Pets [51]	Mean per-class accuracy
	Oxford Flowers-102 [47]	Mean per-class accuracy
	Caltech101 [26]	Mean per-class accuracy
	Stanford Cars [38]	Top-1 accuracy
	FGVC-Aircraft [43]	Mean Per-class accuracy
	Describable Textures (split 1) [20]	Top-1 accuracy
	SUN397 (split 1) [68]	Top-1 accuracy
	Caltech-UCSD Birds [66]	Top-1 accuracy
300 Faces In-the-Wild [59]	$R^2$	
Object detection	VOC2007 [25]	Average Precision [42]
Few-shot classification	Few-Shot CIFAR100 [50]	Average accuracy
	Caltech-UCSD Birds [66]	Average accuracy
	Plant Disease [46]	Average accuracy
	Oxford Flowers-102 [47]	Mean per-class accuracy

**Linear evaluation** We follow the linear evaluation protocol of [15, 30, 37, 40]. Namely, we center-crop and resize the images from the downstream dataset to the size of  $224 \times 224$ , pass them

through the pretrained feature extractor, and obtain the embeddings from the final feature extractor stage. The only exception from this is the CUB dataset [66], where, following [40], for the training images besides the center crop of the image, we also crop the image at its corners and do the same for the horizontal flip of the image (this is known as TenCrop operation<sup>5</sup>).

Having gathered the image features, we minimize the  $l_2$ -regularized cross-entropy objective using L-BFGS on the features of the training images. We select the regularization parameter from between  $[10^{-6}, 10^5]$  using the validation features. Finally, we train the linear classifier on training and validation features with the selected  $l_2$  parameter and report the final performance metric (see Table 5) on the test dataset. We set the maximum number of iterations in L-BFGS as 5000 and use the model trained on training data as initialization for training the final model.

We note that the above linear evaluation procedure is effectively equivalent to training the final layer of a network on non-augmented data, while keeping the remainder of the parameters unchanged.

**Object detection** We closely follow the evaluation protocol of [32]. We train the Faster-RCNN [56] model with the pretrained backbone. Contrary to [32], we do not tune the backbone parameters, in order to better observe the effect of different pretraining methods. We report the Average Precision [42] measured on the VOC test2007 set [25].

**Sensitivity to augmentations** We consider image pairs, where one image is the (center-cropped) original and the second one is augmented by the given augmentation. For each image pair, we extract image features at four stages of the pretrained ResNet-50 backbone [33], as well as the final representation of the projector network. We next calculate cosine similarities between the features of augmented and non-augmented images in the given mini-batch (of size 256). We report the value of the InfoNCE loss [64] calculated on such similarity matrices.

**Dependency of CASSLE projector on conditioning** Similarly to the above experiment, we compare the projector features of augmented and non-augmented image pairs. When computing the features of the augmented image, we supply the projector with the augmentation embedding computed from augmentation parameters corresponding to either this image (true augmentation information) or another, randomly chosen image from the same mini-batch (random augmentation information). We then compute cosine similarities between the original image features and features of the augmented image computed with true/random augmentation information.

## C Additional results and analysis

### C.1 Evaluation

**Rotation prediction** In order to understand whether CASSLE learns to generalize to other types of augmentation, which were not used during pretraining, we inspect the prediction of applied augmentation through the following experiment. We train a linear classifier on top of the pretrained model to indicate whether the image was rotated by 0, 90, 180, or 270 degrees. We formulate the problem as classification due to its cyclic nature and test the model on the datasets used for linear evaluation in Section 4.1 of the main manuscript. We present the results of vanilla, AugSelf [40] and CASSLE variants of self-supervised methods in Table 6. Apart from a few exceptions, CASSLE and AugSelf extensions allow in general for better prediction of rotation than the vanilla SSL methods. Moreover, in the case of SimCLR, CASSLE representation predicts the rotations the most accurately on a vast majority of datasets. This occurs despite the fact, that neither of the methods was trained using rotated images and thus, never explicitly learned the *concept* of rotation. This suggests that CASSLE learns representations which are sensitive to a broader set of perturbations than those whose information had been used in CASSLE’s pretraining.

**Linear evaluation – additional SSL frameworks** We evaluate CASSLE on additional joint-embedding SSL frameworks [32, 30, 18, 72], following the same linear evaluation protocol as in Section 4.1, and present the results in Table 7. In all cases, CASSLE improves the performance of the respective Vanilla approaches. In the case of MoCo-v1 and Barlow Twins, it also achieves

---

<sup>5</sup><https://pytorch.org/vision/main/generated/torchvision.transforms.TenCrop.html>

Table 6: Linear evaluation on downstream task: predicting the rotation (0, 90, 180 or 270 degrees)

Method	C10	C100	Food	Pets	MIT	Flowers	Caltech	Cars	FGVCA	STL10	SUN
<i>SimCLR</i> [15]											
Vanilla	67.93	56.88	68.76	65.07	<b>70.40</b>	24.15	56.81	87.12	98.02	<b>73.90</b>	67.94
AugSelf [40]	75.63	63.08	75.01	57.99	16.54	<b>33.99</b>	39.03	76.11	96.64	67.88	76.60
<b>CASSLE</b>	<b>77.07</b>	<b>70.20</b>	<b>79.55</b>	<b>70.97</b>	68.77	33.08	<b>64.97</b>	<b>95.14</b>	<b>99.46</b>	72.69	<b>78.16</b>
<i>MoCo-v2</i> [32, 17]											
Vanilla	67.96	56.96	75.70	71.27	67.13	<b>58.30</b>	<b>87.33</b>	58.35	93.20	<b>95.44</b>	68.33
AugSelf [40]	<b>74.57</b>	65.87	73.03	<b>77.01</b>	<b>79.75</b>	52.81	58.53	<b>93.07</b>	98.26	77.35	<b>83.66</b>
<b>CASSLE</b>	73.21	<b>69.91</b>	<b>77.31</b>	76.04	76.40	45.11	61.06	90.49	<b>98.56</b>	63.65	76.01
<i>SimSiam</i> [18]											
Vanilla	68.11	64.81	77.35	61.79	<b>79.10</b>	46.33	<b>64.76</b>	80.50	97.48	55.38	74.49
AugSelf [40]	<b>77.00</b>	72.91	73.03	59.18	78.28	<b>49.11</b>	60.86	<b>97.21</b>	<b>99.46</b>	<b>76.68</b>	<b>83.14</b>
<b>CASSLE</b>	72.00	<b>71.38</b>	<b>78.01</b>	<b>85.30</b>	66.80	37.65	61.64	92.04	98.65	63.69	75.86
<i>Barlow Twins</i> [72]											
Vanilla	73.67	64.87	72.85	<b>83.02</b>	70.97	42.56	<b>57.71</b>	83.68	97.93	65.70	76.87
AugSelf [40]	72.79	<b>65.91</b>	74.93	77.76	50.30	30.93	44.31	85.85	98.35	<b>69.68</b>	<b>77.19</b>
<b>CASSLE</b>	<b>74.97</b>	65.15	<b>76.55</b>	77.05	<b>86.49</b>	<b>43.16</b>	53.60	<b>92.92</b>	<b>99.16</b>	55.24	74.97

Table 7: Linear evaluation on downstream classification and regression tasks. CASSLE consistently improves representations formed by vanilla SSL approaches and performs better or comparably to other techniques of increasing sensitivity to augmentations [69, 40, 14].

Method	C10	C100	Food	MIT	Pets	Flowers	Caltech	Cars	FGVCA	DTD	SUN	CUB	300W
<i>MoCo-v1</i> [32] (no projector, $\epsilon$ and $\omega$ joined through addition)													
Vanilla <sup>†</sup>	58.82	28.09	25.90	31.04	47.25	33.29	44.41	5.00	10.98	36.86	19.00	9.16	88.05
AugSelf	64.94	37.01	32.84	33.13	45.95	38.59	45.15	8.33	15.14	40.37	20.48	11.27	88.12
<b>CASSLE</b>	<b>80.53</b>	<b>53.55</b>	<b>52.11</b>	<b>51.94</b>	<b>57.58</b>	<b>60.56</b>	<b>60.33</b>	<b>18.68</b>	<b>28.68</b>	<b>53.94</b>	<b>36.71</b>	<b>18.88</b>	<b>88.21</b>
<i>BYOL</i> [30]													
Vanilla	83.48	60.17	57.79	62.84	75.70	82.47	78.80	38.38	38.16	63.46	46.97	34.12	88.81
AugSelf [40]	<b>85.55</b>	<b>65.03</b>	<b>62.59</b>	<b>64.33</b>	<b>77.48</b>	<b>87.48</b>	81.13	<b>41.06</b>	<b>43.39</b>	64.63	<b>49.31</b>	<b>40.90</b>	89.28
<b>CASSLE</b>	84.20	62.00	57.35	60.97	73.29	85.44	<b>81.52</b>	40.18	42.11	<b>65.59</b>	47.63	33.36	<b>93.03</b>
<i>SimSiam</i> [18]													
Vanilla	86.89	66.33	61.48	65.75	74.69	88.06	84.13	48.20	48.63	65.11	50.60	38.40	89.01
AugSelf [40]	<b>88.80</b>	<b>70.27</b>	<b>65.63</b>	<b>67.76</b>	<b>76.34</b>	<b>90.70</b>	<b>85.30</b>	47.52	<b>49.76</b>	<b>67.29</b>	<b>52.28</b>	<b>45.30</b>	<b>92.84</b>
<b>CASSLE</b>	87.38	67.36	63.27	66.84	75.02	88.95	84.86	<b>48.51</b>	49.35	66.81	51.62	39.47	89.37
<i>Barlow Twins</i> [72]													
Vanilla <sup>†</sup>	85.90	66.10	59.41	61.72	72.30	87.13	81.95	41.54	44.40	65.85	49.18	35.02	89.04
AugSelf [40] <sup>†</sup>	<b>87.28</b>	66.98	60.52	63.96	72.11	86.68	81.73	39.88	44.23	65.21	47.71	37.02	88.88
<b>CASSLE</b>	87.03	<b>67.27</b>	<b>62.19</b>	<b>65.08</b>	<b>72.75</b>	<b>87.99</b>	<b>82.56</b>	<b>41.68</b>	<b>46.63</b>	<b>66.31</b>	<b>50.09</b>	<b>38.25</b>	<b>89.52</b>

stronger performance than AugSelf [40], whereas in the case of self-distillation methods [30, 18], the performances are comparable. We suspect that the lower performance of CASSLE compared to AugSelf with those methods stems from their asymmetric architecture, i.e., distilling the representations between the projector and an additional predictor network. Observe that CASSLE and AugSelf also perform comparably on MoCo-v3, which also utilizes an additional predictor (see Table 1). Perhaps most curiously, CASSLE lends a major performance boost to MoCo-v1 [32]. This is surprising, as the original MoCo-v1 architecture does not utilize a projector network. As such, in this particular case, CASSLE joins the image and augmentation embeddings through element-wise addition. Nevertheless, this simple modulation improves the results by a large margin.



**Few-shot classification** We next benchmark various forms of pretraining on a number of few-shot learning tasks: Few-Shot CIFAR100 (FC100) [50], Caltech-UCSD Birds (CUB) [66], Plant Disease [46]. For the above datasets, we report the performance on 5-way 1-shot and 5-way 5-shot tasks. Moreover, we also report the performance on the 5-shot and 10-shot versions of the Flowers-102 dataset (Flowers) [47]. Following [40], our few-shot models are trained through logistic regression on representations of support images, without fine-tuning. We follow the evaluation protocol of [40]. For the task of 5/10-shot learning of the Flowers dataset [47], we select the subset of the training set with 5/10 examples per class, respectively, and utilize the linear evaluation protocol presented above. For the remaining datasets used for few-shot evaluation, we extract the representations of support and query images with the feature extractor and train a logistic regression model<sup>6</sup>, which we evaluate on the query set. We report the average accuracy from 2000  $N$ -way  $K$ -shot tasks [61] in Table 8. In general, CASSLE improves the performance of the vanilla joint-embedding approaches, but to a lesser extent than AugSelf [40] or AI [14]. The notable exception is Barlow Twins [72], where CASSLE yields the strongest performance boost.

Table 8: Few-shot classification accuracy averaged over 2000 tasks on Few-Shot CIFAR100 (FC100) [50], Caltech-UCSD Birds (CUB) [66], Plant Disease [46], and accuracy on 5-shot and 10-shot versions of Flowers-102 dataset (Flowers) [47]. (N, K) denotes N-way K-shot tasks. The best performance in each group is **bolded**.

Method	FC100		CUB		Plant Disease		Flowers	
	(5,1)	(5,5)	(5,1)	(5,5)	(5,1)	(5,5)	(102, 5)	(102,10)
<i>MoCo v2</i> [32, 17]								
Vanilla	31.67	43.88	41.67	56.92	65.73	84.98	66.83 <sup>†</sup>	78.80 <sup>†</sup>
AugSelf [40]	35.02	48.77	44.17	57.35	71.80	87.81	<b>72.95<sup>†</sup></b>	<b>82.12<sup>†</sup></b>
AI [14]	<b>37.40</b>	48.40	<b>45.00</b>	<b>58.00</b>	<b>72.60</b>	<b>89.10</b>	–	–
LooC [69]	–	–	–	–	–	–	70.90	80.80
<b>CASSLE</b>	35.15	<b>49.30</b>	42.98	55.82	70.74	87.12	72.36	82.07
<i>SimCLR</i> [15]								
Vanilla <sup>†</sup>	34.60	47.21	42.27	54.72	71.12	87.49	70.73	80.72
AugSelf [40] <sup>†</sup>	<b>36.63</b>	<b>49.78</b>	<b>42.88</b>	<b>56.96</b>	<b>74.09</b>	<b>89.72</b>	<b>73.86</b>	82.91
<b>CASSLE</b>	34.82	48.54	41.97	55.84	72.17	88.17	73.23	<b>83.34</b>
<i>Barlow Twins</i> [72]								
Vanilla <sup>†</sup>	38.08	53.93	43.20	61.95	70.98	91.06	75.28	83.43
AugSelf [40] <sup>†</sup>	37.48	<b>54.16</b>	42.50	61.86	71.28	91.16	74.49	83.62
<b>CASSLE</b>	<b>38.58</b>	54.03	<b>43.22</b>	<b>62.65</b>	<b>73.47</b>	<b>92.17</b>	<b>76.62</b>	<b>85.50</b>
<i>SimSiam</i> [18]								
Vanilla	36.19	50.36	45.56	62.48	75.72	89.94	75.53 <sup>†</sup>	85.90
AugSelf [40]	<b>39.37</b>	<b>55.27</b>	<b>48.08</b>	<b>66.27</b>	<b>77.93</b>	<b>91.52</b>	<b>79.67<sup>†</sup></b>	<b>88.30</b>
<b>CASSLE</b>	36.18	50.16	44.93	60.07	76.43	90.82	77.96	86.64

**Fine-tuning** In addition to linear evaluation, we also evaluate the models pretrained with MoCo-v2 under the L2SP fine-tuning paradigm [41] on Caltech-101 [26], CIFAR-10 [39], CUB-200 [66], Food-101 [10], MIT-67 [54], and Pets [51] datasets. We follow the hyperparameters of Li. et. al. [41], i.e.  $\beta = 0.01$ ,  $\alpha \in \{0.001, 0.01, 0.1, 1\}$ , and learning rate  $\in \{0.005, 0.01, 0.02\}$ . We report our results in Table 9. We find that while fine-tuned networks differ in performance by a lesser margin than during linear evaluation, CASSLE-pretrained networks perform favorably in 8 out of 18 cases, more than either vanilla MoCo-v2 or AugSelf.

<sup>6</sup>We use the Logistic Regression implementation from scikit-learn [53].

Table 9: Results of fine-tuning different variants of MoCo-v2 with L2SP protocol [41].

Method	Caltech-101	CIFAR-10	CUB-200	Food-101	MIT-67	Pets
MoCo-v2						
<b>Vanilla</b>	<b>89.80</b>	94.65	56.31	74.36	61.79	82.97
<b>AugSelf</b>	89.16	94.36	<b>56.67</b>	<b>74.94</b>	<b>63.73</b>	<b>83.27</b>
<b>CASSLE</b>	89.27	<b>94.73</b>	55.93	74.07	61.19	82.86
Barlow Twins						
<b>Vanilla</b>	<b>86.54</b>	91.67	48.02	55.68	<b>63.43</b>	77.98
<b>AugSelf</b>	85.82	91.94	48.23	56.35	62.91	77.84
<b>CASSLE</b>	86.01	<b>92.03</b>	<b>54.15</b>	<b>59.83</b>	62.54	<b>78.71</b>
SimCLR						
<b>Vanilla</b>	<b>90.67</b>	94.75	54.55	75.36	63.51	83.65
<b>AugSelf</b>	90.38	94.76	<b>56.36</b>	75.86	62.91	<b>84.25</b>
<b>CASSLE</b>	90.47	<b>95.19</b>	55.65	<b>76.78</b>	<b>63.88</b>	83.51

Table 10: Evaluation of variants of MoCo-v2 on perturbed ImageNet-100 images.

Method	Brightness	Frost	Fog	Snow
<b>Vanilla</b>	85.30	<b>53.70</b>	<b>56.92</b>	31.78
<b>AugSelf</b>	83.64	51.98	53.08	33.80
<b>CASSLE</b>	<b>86.10</b>	50.54	54.22	<b>34.66</b>

**Robustness under perturbations** We next verify the influence of increased sensitivity to augmentations on the robustness of MoCo-v2-pretrained models to perturbations. Following the experimental setup of [40], we train the pretrained networks for classification of ImageNet-100 and evaluate them on weather-corrupted images (fog, frost, snow, and brightness) [34] from the validation set. We report the results in Table 10. We find that the network pretrained with CASSLE achieves the best results when dealing with images perturbed by brightness and snow, whereas vanilla MoCo-v2 performs best on images perturbed by fog and frost.

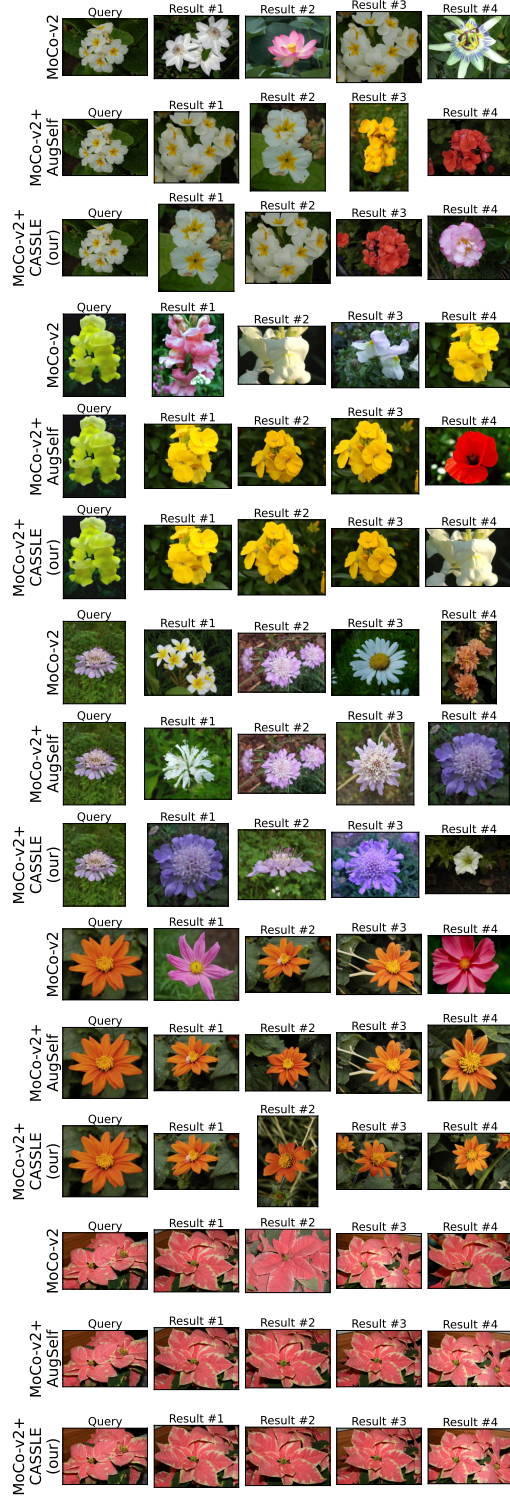
**Image retrieval** Finally, we evaluate the pretrained models on the task of image retrieval. We gather the features of images from the Cars and Flowers test sets and for a given query image, select four images closest to it in terms of the cosine distance of final feature extractor representations. We compare the images retrieved by MoCo-v2, AugSelf [40] and CASSLE in Figure 5. CASSLE selects pictures of cars that are the most consistent in terms of color. In the case of flowers, the nearest neighbor retrieved by the vanilla model is a different species than that of the first query image, whereas both CASSLE and AugSelf select the first two nearest neighbors from the same species but then retrieve images of flowers with similar shapes, but different colors. This again indicates greater reliability of features learned by CASSLE. For subsequent queries, CASSLE and AugSelf retrieve in general more consistently looking images, in particular in terms of color scheme. However, for some distinct images, such as the last presented image of flowers, all methods have retrieved the correct results for the given query.

## C.2 Extended analysis of representations formed by CASSLE

**Analysis of dimensional collapse of representations** Augmentation-invariant SSL models are known to suffer from dimensional collapse of their representations, due to the usage of strong augmentations and implicit regularization [35]. Here, we analyze the effect of CASSLE on this phenomenon. To this end, we compute the embeddings of the ImageNet-100 test dataset with pretrained feature extractors and calculate the empirical eigenspectra of the embeddings produced by each encoder. We next analyze the power-law decay rates ( $\alpha$ ) of eigenspectra [1]. Intuitively, smaller values of  $\alpha$  suggest a dense encoding, while larger values of  $\alpha$  suggest more sparse encoding and rapid decay. We report the calculated coefficients in Table 11. In all analyzed SSL methods,



(a) Cars



(b) Flowers

Figure 5: Image retrieval examples for Cars and Flowers datasets.

except Barlow Twins, the addition of augmentation information by CASSLE leads to a representation whose eigenspectrum decays more rapidly, thus suggesting a lower rank of the effective embedding subspace and as such, greater dimensional collapse. However, as seen in the main text, this does not necessarily lead to degraded performance – indeed, performance on downstream tasks has been previously correlated with how close  $\alpha$  is to 1 [1].

Table 11: Power-law eigenspectrum decay rates ( $\alpha$ ) [1] of embeddings of ImageNet-100 test set produced by differently pretrained feature extractors.

Method	MoCo-v2 [32, 17]	SimCLR [15]	Barlow Twins [72]	SimSiam [18]
Vanilla	0.6013	0.6150	<b>0.5387</b>	0.6365
AugSelf [40]	0.6146	0.6251	0.5201	0.6262
<b>CASSLE</b>	<b>0.6342</b>	<b>0.6908</b>	0.5196	<b>0.6962</b>

We illustrate this further with a Principal Component Analysis of features extracted by different variants of joint-embedding methods illustrated in Figure 6. We extract embeddings of the test ImageNet-100 images and calculate the ratio of variance explained by principal components of embeddings. We find that, in general, representations learned with CASSLE require fewer principal components to explain larger amounts of variance. For example, for MoCo-v2, 90% of variance is explained by 905, 872, and 736 principal components of representations learned by the vanilla approach, AugSelf [40], and CASSLE, respectively. This again suggests that representations learned by CASSLE have lower effective rank compared to other approaches.

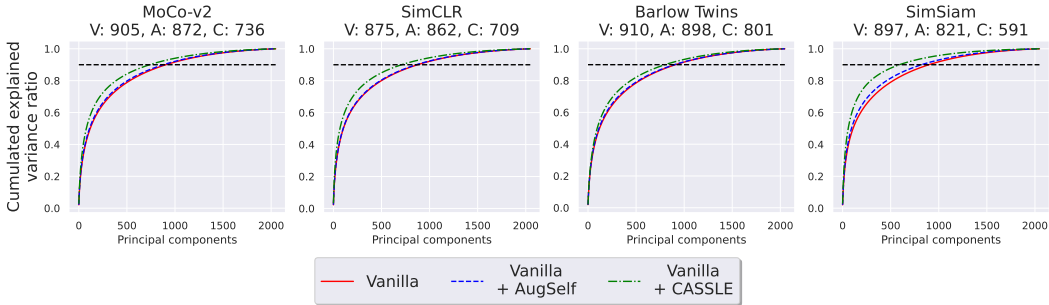


Figure 6: Cumulated explained variance ratio of representations learned by self-supervised models trained in their original forms, as well as with AugSelf [40] and CASSLE extensions. We additionally denote the number of principal components which that explain 90% of the variance of each representation. Models pretrained with CASSLE explain the largest amount of variance with the smallest amount of components, suggesting a larger dimensionality collapse of their representations.

**Analysis of the contrastive learning procedure** We next compare the training of MoCo-v2 [32, 17] with and without CASSLE or AugSelf [40] extensions, and plot the contrastive loss values measured throughout training in the left part of Figure 7, and on the right, the values of losses relative to the baseline MoCo-v2. CASSLE minimizes the contrastive objective faster than the other two variants, in particular early in the training procedure. This suggests that augmentation information provides helpful conditioning for a model not yet fully trained to align augmented image pairs and thus, CASSLE learns to depend on this information.

### C.3 Expanded ablation study results

In order to optimally select the hyperparameters of CASSLE, we train different variants of MoCo-v2+CASSLE and evaluate them on the same classification and regression tasks as in Section 4.1 of the main paper. We rank the models from best to worst performance on each task and report the full results and average ranks in Table 12.

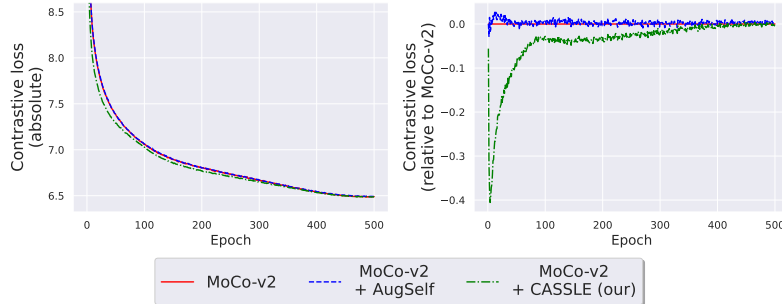


Figure 7: Absolute (left) and relative to Baseline (right) values of contrastive losses of Baseline, AugSelf [40], and CASSLE MoCo-v2 variants, measured during pretraining. CASSLE minimizes the contrastive objective faster than Baseline and AugSelf, in particular early in the training procedure.

We recall the notation used for Augmentation information contents –  $\omega^{\{x,y\}}$  denotes including parameters of augmentations  $\{x, y\}$  in augmentation information vector  $\omega$ . For example,  $\omega^{\{c,j\}}$  denotes  $\omega$  containing cropping and color jittering parameters.

Table 12: Ablation study of CASSLE parameters. The results are computed with MoCo-v2+CASSLE. It is best to condition CASSLE on all available augmentation information. CASSLE yields the best results when implemented by concatenating or adding the augmentation and image embeddings together.

Parameter	C10	C100	Food	MIT	Pets	Flowers	Caltech	Cars	FGVCA	DTD	SUN	CUB	300W	Avg. rank ↓
Augmentation information contents														
$\omega^{\{c\}}$	84.89	62.95	59.74	63.96	72.26	83.55	79.66	38.78	42.03	65.11	48.44	33.86	89.17	4.54
$\omega^{\{c,j\}}$	85.56	64.26	60.35	62.61	71.97	84.73	79.86	38.13	42.17	66.28	48.01	34.24	88.76	4.54
$\omega^{\{c,j,d\}}$	85.87	63.91	61.07	63.51	72.71	86.53	79.51	38.27	42.53	66.70	49.27	35.76	89.11	3.08
$\omega^{\{c,j,b,f\}}$	86.16	64.51	60.80	63.81	72.83	84.66	79.90	38.93	43.02	66.12	48.96	34.40	88.69	2.85
$\omega^{\{c,j,b,f,g\}}$	85.85	64.14	61.24	63.73	72.88	84.50	79.93	38.23	41.28	65.27	48.90	34.47	88.78	3.54
$\omega^{\{c,j,b,f,g,d\}}$	86.99	65.28	61.83	63.51	73.22	86.55	79.87	37.97	41.70	67.18	48.85	36.92	89.03	<b>2.54</b>
Method of conditioning the projector														
<b>Concatenation</b>	86.99	65.28	61.83	63.51	73.22	86.55	79.87	37.97	41.70	67.18	48.85	36.92	89.03	<b>1.92</b>
<b>Addition</b>	86.45	65.40	63.00	65.15	71.34	86.91	79.79	37.83	42.18	66.17	49.28	37.42	88.87	<b>1.92</b>
<b>Multiplication</b>	86.72	66.70	60.65	60.97	64.60	85.17	80.09	33.54	41.56	63.99	47.63	32.15	89.48	2.69
<b>Hypernetwork</b>	84.70	63.55	60.62	64.10	67.16	82.76	78.47	33.39	39.85	66.44	47.43	30.48	89.11	3.46
Depth of the Augmentation encoder (0 denotes concatenating raw $\omega$ to e)														
<b>0</b>	86.53	65.99	62.54	61.72	69.04	85.46	80.74	36.44	41.91	65.64	48.55	33.88	92.72	3.38
<b>2</b>	86.57	64.80	61.85	62.68	72.79	86.31	79.93	37.85	42.87	66.32	49.23	35.39	88.86	3.08
<b>4</b>	86.32	65.16	61.98	64.93	72.64	86.49	79.75	38.64	41.46	66.91	49.71	36.56	89.27	2.38
<b>6</b>	86.99	65.28	61.83	63.51	73.22	86.55	79.87	37.97	41.70	67.18	48.85	36.92	89.03	<b>2.15</b>
<b>8</b>	85.47	64.88	61.49	63.13	72.41	85.65	78.22	37.82	40.71	66.70	49.21	36.09	88.90	4.00
Hidden size of the Augmentation encoder														
<b>16</b>	84.51	63.40	61.38	62.31	71.61	85.40	78.96	37.53	41.84	66.54	48.68	35.54	88.78	5.54
<b>32</b>	85.43	63.94	61.93	64.18	72.05	85.67	79.80	37.86	41.52	67.13	48.71	35.64	88.67	4.38
<b>64</b>	86.99	65.28	61.83	63.51	73.22	86.55	79.87	37.97	41.70	67.18	48.85	36.92	89.03	<b>2.54</b>
<b>128</b>	86.24	64.66	61.95	64.25	72.12	86.72	79.56	37.79	42.71	67.61	49.52	36.87	88.99	2.62
<b>256</b>	86.23	65.63	61.77	61.79	72.03	85.69	80.38	37.86	40.94	67.07	49.59	37.00	89.37	3.31
<b>512</b>	85.77	66.05	62.21	64.55	72.45	86.38	80.06	37.91	41.94	66.22	49.35	36.24	88.87	2.69
Impact of utilizing color difference information during pretraining														
<b>AugSelf</b> $\omega^{\{c,j\}}$	85.26	63.90	60.78	63.36	73.46	85.70	78.93	37.35	39.47	66.22	48.52	37.00	<b>89.49</b>	3.07
CASSLE $\omega^{\{c,j,b,f,g\}}$	85.85	64.14	61.24	63.73	72.88	84.50	<b>79.93</b>	38.23	41.28	65.27	48.90	34.47	88.78	2.64
AugSelf $\omega^{\{c,j,d\}}$	84.95	64.06	61.53	63.06	<b>73.52</b>	86.25	77.38	36.00	<b>42.54</b>	66.33	48.65	<b>37.40</b>	88.36	2.71
<b>CASSLE</b> $\omega^{\{c,j,b,f,g,d\}}$	<b>86.32</b>	<b>65.29</b>	<b>61.93</b>	<b>63.86</b>	72.86	<b>86.51</b>	79.63	<b>38.82</b>	42.03	<b>66.54</b>	<b>49.25</b>	36.22	88.93	<b>1.57</b>

## D Implementation details

We implement CASSLE in the PyTorch framework [52], building upon the codebase of [40]. The anonymized version of our code is available at <https://anonymous.4open.science/r/CASSLE-037C/README.md>.